Experimental Demonstration of Accurate Noncontact Measurement of Arterial Pulse Wave Displacements Using 79-GHz Array Radar

Yuji Oyamada, Takehito Koshisaka, and Takuya Sakamoto, *Senior Member, IEEE*

***Abstract*—In this study, we present a quantitative evaluation of the accuracy of simultaneous array-radar-based measurements of the displacements caused at two parts of the human body by arterial pulse wave propagation. To establish the feasibility of accurate radar-based noncontact measurement of this pulse wave propagation, we perform experiments with four participants using a 79-GHz millimeter-wave ultra-wideband multiple-input multiple-output array radar system and a pair of laser displacement sensors. We evaluate the accuracy of the pulse wave propagation measurements by comparing the displacement waveforms that are measured using the radar system with the corresponding waveforms that are measured using the laser sensors. In addition, to evaluate the estimates of the pulse wave propagation channels, we compare the impulse response functions that are calculated from the displacement waveforms obtained from both the radar data and the laser data. The displacement waveforms and the impulse responses both demonstrated the good agreement between the results of the radar and laser measurements. The normalized correlation coefficient between the impulse responses obtained from the radar and laser data on average was as high as 0.97 for the four participants. The results presented here strongly support the feasibility of accurate radar-based noncontact measurement of arterial pulse wave propagation.**

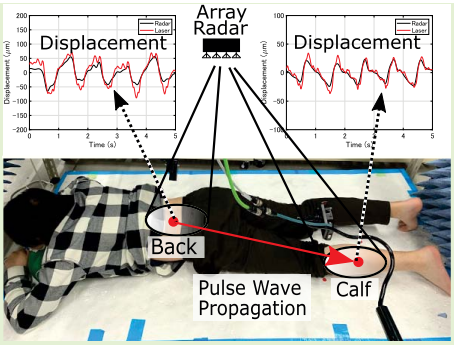

***Index Terms*— Array radar, arterial pulse wave, impulse response, laser displacement sensor.**

I. Introduction

THE arterial pulse wave velocity (PWV), the pulse arrival time (PAT), and the pulse transit time (PTT) are all known indicators of a variety of cardiovascular diseases [1]–[5]. The PAT is the time difference between the occurrence of the R wave in an electrocardiogram (ECG) and the time at which the related pulse arrives at a specific body part; the PTT is the time difference between two PATs measured at different body parts; and the PWV can then be calculated by dividing the distance between the two body parts by either the PAT or the PTT. In clinical practice, the volume change caused by the pulse wave is measured at multiple body sites to estimate the PWV. For example, the baPWV (brachial-ankle PWV) method, which is used to detect the progress of arteriosclerosis, measures the PWV using cuffs attached to all four of the patient's limbs.

Another application of the PAT and PTT is estimation of the systolic blood pressure (BP) without use of cuffs. If a patient's BP must be monitored constantly, a conventional sphygmomanometer with inflatable cuffs is cumbersome to wear and involves uncomfortable physical restraint for the patient. To resolve these issues, cuffless BP measurement techniques have been studied and the most promising approach involves use of the relationship between the BP and the PAT/PTT [6]. Numerous promising results on BP estimation using cuffless systems have been reported in the literature [7], [8].

The PAT can be measured using a combination of ECG and photoplethysmograph (PPG) sensors [9]–[14]. Ma and Zhang [10] and Wong *et al.* [11] studied the accuracy of PAT-based BP measurements. Zheng *et al.* [12] evaluated the performance of PAT-based BP measurements using 24 h data. Thomas *et al.* [13] developed a compact wristwatch-like

Manuscript received November 18, 2020; revised December 23, 2020 and January 14, 2021; accepted January 14, 2021. Date of publication January 18, 2021; date of current version March 5, 2021. This work was supported in part by the Japan Society for the Promotion of Science (JSPS) KAKENHI under Grant 19H02155, in part by the Japan Science and Technology Agency (JST) Precursory Research for Embryonic Science and Technology (PRESTO) under Grant JPMJPR1873, and in part by JST Center of Innovation (COI) under Grant JPMJCE1307. The associate editor coordinating the review of this article and approving it for publication was Prof. Piotr J. Samczynski. *(Corresponding author: Takuya Sakamoto.)*

The authors are with the Department of Electrical Engineering, Graduate School of Engineering, Kyoto University, Kyoto 615-8510, Japan (e-mail: sakamoto.takuya.8n@kyoto-u.ac.jp).

Digital Object Identifier 10.1109/JSEN.2021.3052602

wearable device that contained both ECG and PPG sensors. Zheng *et al.* [14] also developed a wristwatch-like wearable system. These systems, however, suffered from an error caused by the uncertainty of the pre-ejection period, which is defined as the time between the onset of the QRS complex and the beginning of ventricular ejection and is known to vary from beat to beat. To avoid this pre-ejection period-related error, the PTT should be measured rather than the PAT [15].

Multiple PPG sensors are often used to perform PTT measurements and these sensors are attached to multiple parts of the patient's body with known distances between them [15]–[17]. For example, PPG sensors have previously been placed on three sites on the patient's head [15], on a patient's wrist and finger [16], and on a patient's finger and foot [17]. Martin *et al.* [17] developed a BP measurement system that resembles a weight scale and comprises various sensors, including an ECG sensor, a finger PPG sensor, a foot PPG sensor, a ballistocardiography sensor, and an impedance cardiography (ICG) sensor. Other sensor types have been also used to monitor the PTT [18]–[21]. Foo *et al.* [18] used a PPG sensor and a phonocardiogram (PCG) sensor; Hsu and Young [19] used microelectromechanical system pressure sensors; Lee *et al.* [20] used a PPG sensor and a magneto-plethysmograph sensor; and Heydari *et al.* [21] used an ECG sensor and bio-impedance sensors to measure the PTT.

However, noncontact sensing is preferred to use of these contact-type sensors because it enables provision of an unobtrusive health monitoring system that can record the PTT/PWV data continuously over long periods. Microwave and millimeter-wave radar systems are particularly promising options for these applications because radar waves can penetrate through both clothing and comforters and can thus measure the physiological signals accurately. There have been several previous reports of radar-based cuffless measurements of pulse wave propagation [22]–[28]. Lin *et al.* [22] measured the PTT using a 300-MHz radar system with an antenna pair. Buxi *et al.* used configurations that included a 1-GHz continuous-wave (CW) radar system with ICG, ECG, PCG, and piezoelectric sensors [23], a 1.1-GHz CW radar system with ICG sensors [24], and a 2.4-GHz CW radar system with ICG, ECG, and PCG sensors [25] to perform PTT measurements. Ebrahim *et al.* [26], [27] measured the PTT using a 900-MHz radar system along with ECG and PCG sensors. Kuwahara *et al.* measured the PTT using a radar system and a piezoelectric pressure sensor attached to the patient's finger [28]. Although radar systems were used in all these previous studies [22]–[28], they also required supplementary contact sensors in addition to the radar system, which means that these systems cannot achieve unobtrusive patient monitoring.

Previous studies on PTT measurement that used radar systems alone have also been reported [29]–[34]. Tao *et al.* estimated the PWV using a radar system placed on the patient's upper arm and left ankle [29]. Tang *et al.* [30] measured the PTT by measuring the displacement of the patient's arm and chest simultaneously using a radar system that the patient wore on their wrist. Lauteslager *et al.* [31] measured the PTT by contacting six parts of the patient's body sequentially using a radar system. Although these studies [29]–[31] did measure the PTT using radar systems only, the radar antennas were placed in close contact with the body surface and thus could not be considered to be noncontact measurements. Vasireddy *et al.* [32] measured the PTT and PWV by placing two radar systems approximately 15 cm from the surface of the patient's chest and from their right groin. Lu *et al.* [33] measured the PWV by placing two radar systems close to the patient's chest and calf. Although the pulse waves were measured via noncontact measurements using multiple radar systems in these studies, the position and posture of the target patient required careful adjustment in each case. In contrast, Michler *et al.* [34] measured the PWV using only a single phased array radar system by forming beams that were directed alternately into two locations in the patient's abdomen. This method required adjustment of the transmission direction according to the position of the target patient.

TABLE I
PARAMETERS OF THE ARRAY RADAR SYSTEM

Modulation	FMCW
Center frequency	79 GHz
Wavelength	3.8 mm
99%-Bandwidth	3.9 GHz
Range resolution	43 mm
Slow-time sampling interval	100 ms
Number of transmitting elements	3
Number of receiving elements	4
Number of virtual elements	12
Virtual element spacing	1.9 mm

In this study, we use a millimeter-wave (MMW) ultra-wideband (UWB) multiple-input multiple-output (MIMO) array radar system to measure two body parts on each of four participants to estimate both their body displacements and the arterial pulse wave propagation. We then evaluate the accuracy of these radar-based measurements by comparing the results with reference data that were obtained using laser displacement sensors. The pulse wave propagation channel is evaluated quantitatively in terms of its impulse response, which is calculated based on the estimated displacement waveforms from the two body parts. Although our previous study [35] indicated the possibility of array-radar-based pulse wave propagation measurement, the accuracy of these measurements has not been evaluated experimentally to date. To the extent of the authors' knowledge, this study is the first to evaluate the accuracy of radar-based noncontact measurements of arterial pulse wave propagation quantitatively. We demonstrate the effectiveness of our proposed system by using an array radar system to perform noncontact experimental measurements of pulse wave propagation.

II. EXPERIMENTAL SETUP WITH ARRAY RADAR AND LASER DISPLACEMENT SENSORS

We conduct the experiments using an array radar system and a pair of laser displacement sensors simultaneously to evaluate the accuracy of the radar-based pulse wave measurements. Note that the laser displacement sensors are only used to evaluate the accuracy of the radar-based measurements. The parameters of the array radar system and the laser displacement sensors are given in Tables I and II, respectively.

TABLE II
PARAMETERS OF THE LASER DISPLACEMENT SENSORS

Measurement principle	triangulation
Measurable distance	150 ± 40 mm
Spot size (diameter)	120 μm
Repeatability	0.2 μm
Wavelength	655 nm
Sampling interval	500 μs

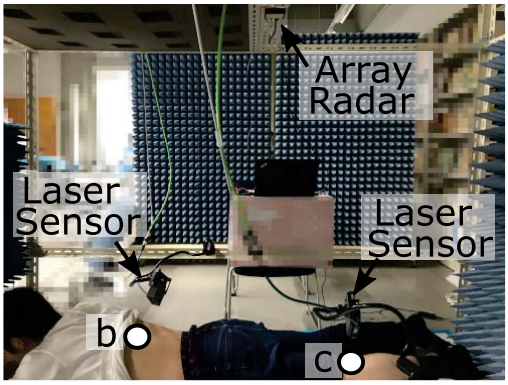

Fig. 1. Measurement setup with a participant shown lying in a prone position on a bed. Two body parts (marked b and c in the image) were measured using both the array radar system and the laser displacement sensors.

TABLE III
BIOMETRIC INFORMATION OF PARTICIPANTS

Participant	A	B	C	D
Age	22	23	22	22
Sex	M	M	M	M
Weight (kg)	58	55	53	59
Height (cm)	165	166	169	172
BMI (kg/m^2)	21.3	20.0	18.6	19.9
Blood pressure (mmHg)	126/85	115/80	111/77	135/90
Heart rate (bpm)	68	63	58	64

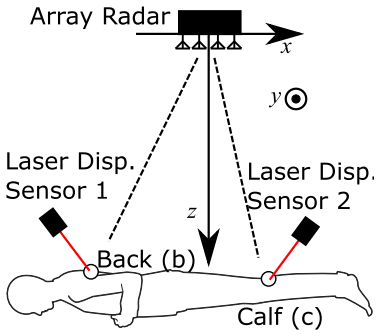

Fig. 2. Schematic of the measurement setup with the array radar system mounted above a participant lying in a prone position.

We use a 79-GHz MMW UWB MIMO array radar system. This system is a frequency-modulated CW (FMCW) radar system with transmit power of 9 dBm, effective isotropic radiated power (EIRP) of 20 dBm, a center frequency of 79 GHz, a center wavelength of $\lambda = 3.8$ mm, and an occupied bandwidth of 3.9 GHz. The beamwidths of the individual elements in the radar array are $\pm 4°$ and $\pm 35°$ in the E- and H-planes, respectively. These beamwidths result in a beam footprint size of 17.8 $\times$ 16.8 cm at a distance of 1.2 m from the array because the 12-element uniform half-wavelength linear array has a half-power beamwidth of $\pm 4.2°$ in the H-plane, which is explained in the Appendix. The radar array is composed of a MIMO array that contains three transmitting and four receiving elements, with spacings between the transmitting elements and between the receiving elements of 7.6 mm (2λ) and 1.9mm ($\lambda/2$), respectively. If we assume that the distance between the array and the targets is much greater than the array aperture size and also assume that the mutual coupling between the array elements is negligible, then the MIMO array can be approximated using a virtual array with elements arranged in a straight line at equal intervals. Specifically, the array used in this study can be approximated using a 12-element virtual linear array with half-wavelength element spacings.

A photograph of the experimental scene with a participant lying on a Styrofoam bed in a prone position is shown in Fig. 1. We conducted the experiments with four participants, who are named A, B, C and D here. All participants are healthy adults and their biometric information is summarized in Table III. The BPs and heart rates of all participants were measured during the experiments. A pair of laser displacement sensors were placed 150 mm from the back and the calf of each participant (Fig. 2). We confirmed that the radar system and the laser sensors both measured almost exactly the same spots (on the back and the calf of each participant), which enables evaluation of the accuracy of the measurements of the body displacements at these two body parts simultaneously. During these experiments, the participants were asked to hold their breath to ensure that their respiration did not affect the measurements.

To measure the displacements that occur at two body parts simultaneously, a beamformer method is used to process the array radar data. For an array that contains K (virtual) elements, the signal $s_i(t, r)$ is received using the i-th element ($i = 1, 2, \cdots, K$), where t is the slow time and $r = ct'/2$ is the range for the fast time t' and the speed of light c. A signal vector $\boldsymbol{s}'(t, r)$ is defined as $\boldsymbol{s}'(t, r) = [s_1(t, r), s_2(t, r), \cdots, s_K(t, r)]^{\mathrm{T}}$, where the superscripted T represents a transpose operator. The static clutter is then suppressed by subtracting the time-averaged profile from the signal vector, that is $\boldsymbol{s}(t, r) = \boldsymbol{s}'(t, r) - (1/T)\int_0^T \boldsymbol{s}'(t, r)\mathrm{d}t$, where T is the total measurement time. A target range r_0 is then selected where $r_0 = \arg\max_r \int_0^T |\boldsymbol{s}(t, r)|^2 \mathrm{d}t$. The signals $\boldsymbol{s}(t, r_0)$ are then processed for the selected range r_0 only. Hereafter, we omit r_0 for simplicity as $\boldsymbol{s}(t) = \boldsymbol{s}(t, r_0)$.

The origin of the xyz coordinates is located at the center of the virtual array. We also assume that the array baseline is located on the x-axis, the array is located in the xy plane, and the downward vertical direction is represented by the z axis (Fig. 2). The beamformer method uses a weight $w_i = \mathrm{e}^{-\mathrm{j}(2\pi x_i/\lambda)\sin\theta}$, where λ is the wavelength, x_i ($i = 1, 2, \cdots, K$) is the distance from the center of the array to the k-th element, and θ is the direction of arrival (DOA). Using a mode vector $\boldsymbol{a}(\theta) = [w_1, w_2, \ldots, w_K]^{\mathrm{T}}$, the DOAs θ_j ($j = 1, 2, \cdots M$) can be estimated based on the dominant peaks of the spatial spectrum:

$$P_{\mathrm{BF}}(\theta) = \int |\boldsymbol{a}^{\mathrm{H}}(\theta)\boldsymbol{s}(t)|^2 \mathrm{d}t, \tag{1}$$

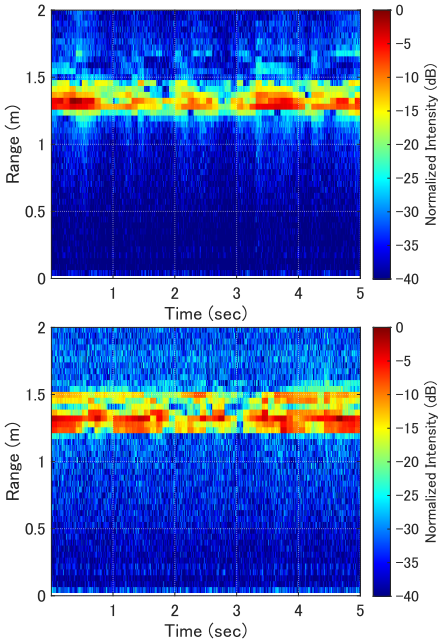

Fig. 3. Range profiles $|s(t, r)|^2$ for participants A (top) and B (bottom).

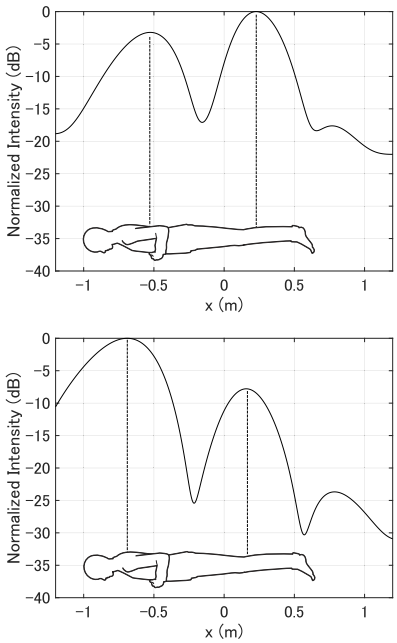

Fig. 4. Cross-range profiles for participants A (top) and B (bottom), where the approximate body size and position of each target person are also displayed.

where M is the number of echoes and the superscripted H represents a complex-conjugate transpose operator. The j-th echo $u_j(t)$ arriving from the angle θ_j is estimated using $u_j(t) = \boldsymbol{a}^{\mathrm{H}}(\theta_j)\boldsymbol{s}(t)$, and the skin displacement $d_i(t) = (\lambda/4\pi)\angle u_i(t)$ is also estimated, where $\angle$ denotes the phase of a complex number. In this study, we focus specifically on two dominant echoes, denoted by $u_1(t)$ and $u_2(t)$, that arrive from two parts of the participant's body and estimate the corresponding displacement waveforms $d_1(t)$ and $d_2(t)$.

III. Comparison of Pulse Wave Waveforms Measured Using Radar and Laser Sensors

The upper and lower panels of Fig. 3 show the range profiles $|s(t, r)|^2$ obtained for participants A and B, respectively, after DC suppression. In this figure, time-changing echoes are observed in the range between 1.2 and 1.5 m. Because the radar has high range resolution, the echoes from the target participant can be separated from the majority of the undesired echoes coming from the background objects in each case. We then select a range r_0 and obtain a signal vector $\boldsymbol{s}(t)$ using the process explained in Section II.

Next, we apply the beamformer method to $\boldsymbol{s}(t)$ to obtain an angular profile $P_{\mathrm{BF}}(\theta)$ and then convert this profile into a cross-range profile $P(x) = P_{\mathrm{BF}}(\sin^{-1}(x/r_0)))$. Two examples of the cross-range profile $P(x)$ that were obtained for participants A and B are shown in Fig. 4, where the approximate heights and positions of the two participants are displayed for the convenience of the reader. The images show that the two dominant peaks in each profile correspond approximately to the echoes returning from the back and the leg of each participant. Similar profiles were also obtained for participants C and D. The proposed method detects the two dominant peaks in the cross-range profile and estimates the reflection points $x_1 = r_0 \sin\theta_1$ and $x_2 = r_0 \sin\theta_2$ $(\theta_1 < \theta_2)$, which are then used to estimate the displacements $d_1(t)$ and $d_2(t)$ that occurred at the two body parts.

The displacement waveforms of the back and calf of participant A were estimated as shown in Fig. 5, where the black and red lines represent the displacements that were measured using the radar system and the laser sensors, respectively. The sampling frequencies used for the radar system and the laser sensors were 10 Hz and 2 kHz, respectively. To ease the process of comparison between the radar and laser signals, which were sampled at different frequencies, we applied a cubic spline interpolation to the radar signals; this caused the sampling frequency of the radar data to match that of the laser data. These displacements are denoted by $d_{\mathrm{b}}^{(\mathrm{R})}(t)$, $d_{\mathrm{c}}^{(\mathrm{R})}(t)$, $d_{\mathrm{b}}^{(\mathrm{L})}(t)$, and $d_{\mathrm{c}}^{(\mathrm{L})}(t)$, where the back and the calf are denoted by the subscripts b and c and the data measured using the radar system and the laser sensors are denoted by the superscripts (R) and (L), respectively. Note that both $d_{\mathrm{b}}^{(\mathrm{R})}(t) = d_1(t)$ and $d_{\mathrm{c}}^{(\mathrm{R})}(t) = d_2(t)$ hold here. As an additional example, the corresponding sets of waveforms for participant B are displayed in Fig. 6. Although some differences can be seen among the details of these waveforms, the overall waveforms measured using the radar system and the laser sensors resemble each other for both participants A and B.

To evaluate the similarities between the displacement waveforms measured using the radar system and the laser sensors quantitatively, we calculate a normalized cross-correlation function $C(\tau)$ between the displacement waveforms at the backs of the participants as:

$$C(\tau) = (1/C_0(\tau)) \int_0^{T'} d_{\mathrm{b}}^{(\mathrm{R})}(t) d_{\mathrm{b}}^{(\mathrm{L})}(t+\tau)\mathrm{d}t, \qquad (2)$$

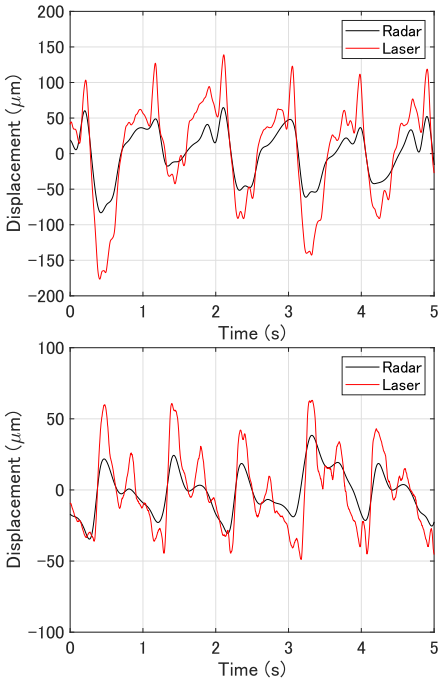

Fig. 5. Displacement waveforms of the back (top) and calf (bottom) measured using the radar system and the laser sensors for participant A.

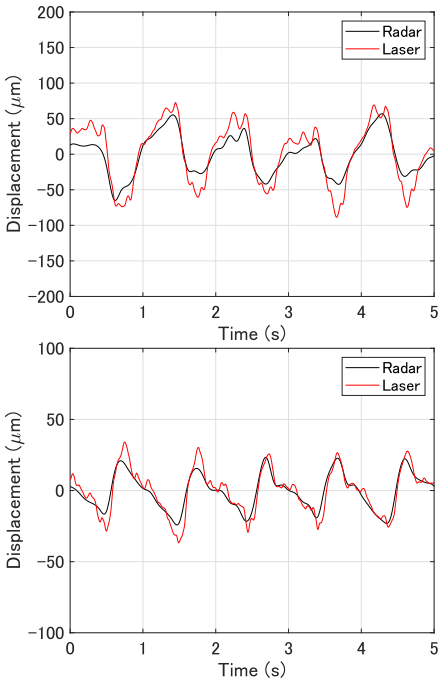

Fig. 6. Displacement waveforms of the back (top) and calf (bottom) measured using the radar system and the laser sensors for participant B.

where τ is the time lag and $C_0(\tau)$ is set as

$$C_0(\tau) = \sqrt{\int_0^{T'} |d_{\rm b}^{\rm (R)}(t)|^2 {\rm d}t \int_0^{T'} |d_{\rm b}^{\rm (L)}(t+\tau)|^2 {\rm d}t} \qquad (3)$$

to normalize $C(\tau)$ ($|C(\tau)| \leq 1$). In the ideal case where $d_{\rm b}^{\rm (R)}(t) = d_{\rm b}^{\rm (L)}(t)$, $C(0) = 1$ holds. Similarly, the normalized cross-correlation function is calculated using the displacement waveforms $d_{\rm c}^{\rm (R)}(t)$ and $d_{\rm c}^{\rm (L)}(t)$ from the calves of the participants.

TABLE IV
MAXIMUM CROSS-CORRELATION $C(\tau_{\rm max})$ AND TIME LAG $\tau_{\rm max}$ FOR THE FOUR PARTICIPANTS

Participant	Body part	$\tau_{\rm max}$	$C(\tau_{\rm max})$
A	Back	0	0.96
	Calf	8.5 ms	0.87
B	Back	0	0.94
	Calf	23.0 ms	0.95
C	Back	0	0.99
	Calf	5.5 ms	0.93
D	Back	0	0.91
	Calf	0.8 ms	0.92

Fig. 8 shows the normalized cross-correlation function $C(\tau)$ characteristics for participants A and B. The figure shows that $C(\tau)$ is quasiperiodic because of the quasiperiodicities of the displacement waveforms $d_{\rm b}^{\rm (R)}(t)$, $d_{\rm b}^{\rm (L)}(t)$, $d_{\rm c}^{\rm (R)}(t)$, and $d_{\rm c}^{\rm (L)}(t)$. We calculate the local maximum of $C(\tau)$, subject to the condition that $|\tau| \leq T_0/2$, where T_0 is the heartbeat interval. Table IV presents the local maximum value $C_{\rm max} = \max_{|\tau| \leq T_0/2} C(\tau)$ and the time lag $\tau_{\rm max} = \arg\max_{|\tau| \leq T_0/2} C(\tau)$ for each of the four participants, where the condition $\tau_{\rm max} = 0$ is imposed for the back in each case because an unknown time offset exists between the radar system and the laser sensors, which are not synchronized. However, imposing $\tau_{\rm max} = 0$ for the back does not affect the overall accuracy evaluation because the propagation channel is dependent on the time difference between the displacements at the two body parts; the time lag error is determined using only $\tau_{\rm max}$ from the calf in each case.

The upper panel in Fig. 7 shows the scatter diagram for the displacements $d_{\rm b}^{\rm (R)}(t_i)$ and $d_{\rm b}^{\rm (L)}(t_i)$ ($i = 1, 2, \cdots, L$) of the back of participant A; the lower panel in Fig. 7 shows the corresponding scatter diagram for the calf of participant A, where the i-th sampling time is $t_i = i\,\Delta t$ with $\Delta t = 25$ ms and $L = 241$. Next, we apply principal component analysis (PCA) to the covariance matrices $M_{\rm b}$ and $M_{\rm c}$, where $M_{\rm b}$ is calculated using $d_{\rm b}^{\rm (R)}$ and $d_{\rm b}^{\rm (L)}$ as follows:

$$M_{\rm b} = \frac{1}{L-1} \sum_{i=1}^{L} \begin{bmatrix} d_{\rm b}^{\rm (R)}(t_i)^2 & d_{\rm b}^{\rm (R)}(t_i) d_{\rm b}^{\rm (L)}(t_i) \\ d_{\rm b}^{\rm (L)}(t_i) d_{\rm b}^{\rm (R)}(t_i) & d_{\rm b}^{\rm (L)}(t_i)^2 \end{bmatrix}, \qquad (4)$$

and $M_{\rm c}$ is calculated in a similar manner using $d_{\rm c}^{\rm (R)}$ and $d_{\rm c}^{\rm (L)}$. For participant A, the eigenvalues $\sigma_{\rm max}$ and $\sigma_{\rm min}$ ($\sigma_{\rm max} \geq \sigma_{\rm min}$) of the matrices $M_{\rm b}$ and $M_{\rm c}$ are calculated; the square roots of these eigenvalues are $\sqrt{\sigma_{\rm max}} = 78.9$ μm and $\sqrt{\sigma_{\rm min}} = 8.5$ μm for $M_{\rm b}$, and $\sqrt{\sigma_{\rm max}} = 29.8$ μm and $\sqrt{\sigma_{\rm min}} = 6.8$ μm for $M_{\rm c}$. The proportions of variance of the first principal component $p_{\rm v} = \sigma_{\rm max}/(\sigma_{\rm max} + \sigma_{\rm min})$ were 98.8% and 95.0% for $M_{\rm b}$ and $M_{\rm c}$, respectively. The same analysis was carried out for all participants and the results are summarized in Table V. The average proportions of variance of the first principal component $p_{\rm v}$ were 97.9% and 96.4% for the back and the calf, respectively, indicating successful radar measurement of the pulse wave displacements.

Fig. 7 also shows ellipses in red with semi-major and semi-minor axes that are equal to $\sqrt{\sigma_{\rm max}}$ and $\sqrt{\sigma_{\rm min}}$,

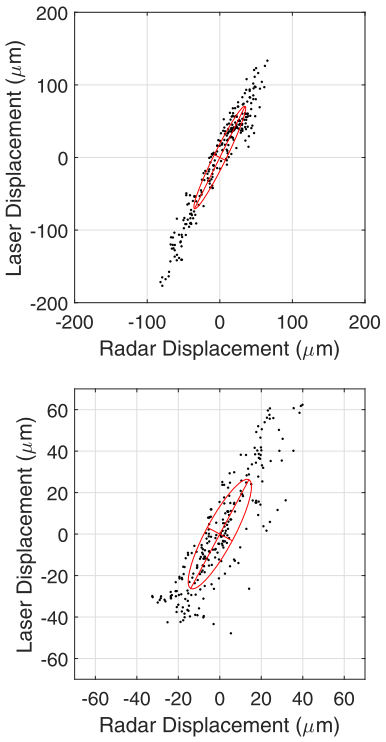

Fig. 7. Scatter diagrams of the displacements measured using the radar and laser sensors for the back (top) and the calf (bottom) of participant A.

TABLE V
PCA RESULTS FOR DISPLACEMENTS MEASURED USING RADAR AND LASER SENSORS

Participant	Body part	$\sqrt{\sigma_{\max}}$	$\sqrt{\sigma_{\min}}$	p_{v}	ψ
A	Back	78.9 μm	8.5 μm	98.8%	63.7°
	Calf	29.8 μm	6.8 μm	95.0%	61.9°
B	Back	44.2 μm	6.6 μm	97.8%	61.2°
	Calf	17.3 μm	3.3 μm	96.4%	45.8°
C	Back	75.0 μm	6.3 μm	99.3%	52.5°
	Calf	27.5 μm	4.9 μm	97.0%	57.5°
D	Back	64.2 μm	13.4 μm	95.8%	41.7°
	Calf	23.3 μm	4.1 μm	97.0%	61.0°

respectively, and the major axis of each ellipse is oriented parallel to the eigenvector $[\cos\psi, \sin\psi]^{\mathrm{T}}$ of the first principal component. The results for the angle of the eigenvector ψ of the first principal component are summarized in Table V, where the average ψ values were 54.8° and 56.6° for the back and the calf, respectively; this indicates that the radar measurements underestimate the displacements by factors of $\tan\psi = 1.4$ and 1.5 on average for the back and the calf, respectively. Note that these factors do not affect the normalized waveforms.

Next, we calculate the root-mean-square (rms) errors e_{b} and e_{c} between the pulse wave displacements, which are expressed in the forms of $e_{\mathrm{b}}^2 = (1/T)\int_0^T |d_{\mathrm{b}}^{(\mathrm{R})}(t) - d_{\mathrm{b}}^{(\mathrm{L})}(t)|^2 \mathrm{d}t$ and $e_{\mathrm{c}}^2 = (1/T)\int_0^T |d_{\mathrm{c}}^{(\mathrm{R})}(t) - d_{\mathrm{c}}^{(\mathrm{L})}(t)|^2 \mathrm{d}t$, respectively. The rms error results for all participants are shown in Table VI. The average rms errors for the back and the calf were 24.1 and 10.1 μm, respectively.

The discrepancy between the displacement waveforms measured using the radar and laser systems can be explained by the difference between the spot sizes of the two sensor

TABLE VI
RMS ERRORS e_{b} AND e_{c} FOR ALL PARTICIPANTS

Participant	e_{b}	e_{c}
A	37.6 μm	14.4 μm
B	19.7 μm	5.4 μm
C	15.2 μm	10.6 μm
D	23.9 μm	10.0 μm
Average	24.1 μm	10.1 μm

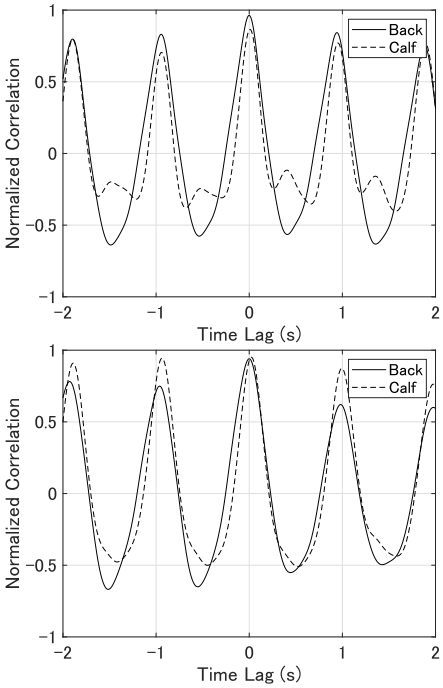

Fig. 8. Correlation function $C(\tau)$ of $d_{\mathrm{b}}^{(\mathrm{L})}(t)$ and $d_{\mathrm{b}}^{(\mathrm{R})}(t)$ (back, solid line); and correlation function $C(\tau)$ of $d_{\mathrm{c}}^{(\mathrm{L})}(t)$ and $d_{\mathrm{c}}^{(\mathrm{R})}(t)$ (calf, broken line) for participants A (top) and B (bottom).

types. The beam spot sizes of the radar and laser sensors are 170 mm and 0.12 mm, respectively; this means that the laser displacement sensors measure the local displacement, whereas the radar system measures the displacement averaged over the beam footprint. Despite this difference, the average value of the correlation coefficient between the displacement waveforms for the radar system and the laser sensors was as high as 0.94. We should also note here that the precision of the evaluation of the correlation coefficients mentioned above can be affected by the interpolation process applied to the radar signals. In future work, our next step will be to take the above effects into account to enable more precise evaluation of the accuracy.

Next, to analyze the pulse wave propagation, we determine the impulse response of a linear time-invariant system that is used to model the pulse wave propagation. The impulse response is approximated using a Wiener filter as:

$$g(\tau) = \int_{-\infty}^{\infty} \frac{\int_{-\infty}^{\infty} d_{\mathrm{c}}(t)\mathrm{e}^{-\mathrm{j}\omega t}\mathrm{d}t \int_{-\infty}^{\infty} d_{\mathrm{b}}(t)\mathrm{e}^{\mathrm{j}\omega t}\mathrm{d}t}{\left|\int_{-\infty}^{\infty} d_{\mathrm{b}}(t)\mathrm{e}^{-\mathrm{j}\omega t}\mathrm{d}t\right|^2 + \eta^2} \mathrm{e}^{\mathrm{j}\omega\tau}\mathrm{d}\omega, \quad (5)$$

where the superscripts (R) and (L) are omitted for simplicity. The parameter η is determined as:

$$\eta = \eta_0 \max_{\omega} \left| \int_{-\infty}^{\infty} d_{\mathrm{b}}(t)\mathrm{e}^{-\mathrm{j}\omega t}\mathrm{d}t \right|, \quad (6)$$

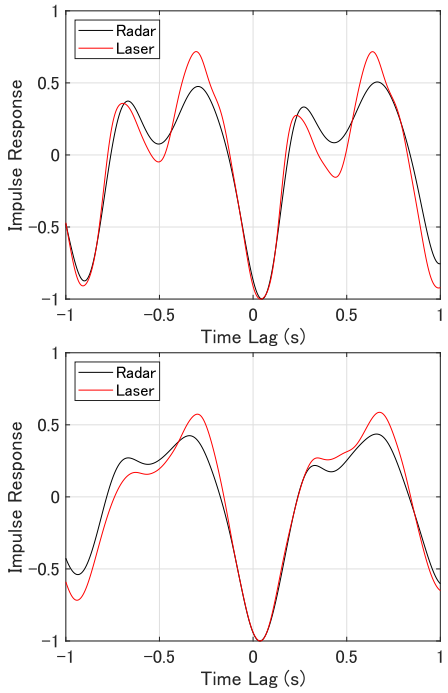

Fig. 9. Impulse responses $g_{\mathrm{R}}(t)$ and $g_{\mathrm{L}}(t)$ representing pulse wave propagation between the back and the calf for participants A (top) and B (bottom).

where $\eta_0 = 0.5$ was selected empirically. The impulse response that was obtained using $d_{\mathrm{b}}^{(\mathrm{R})}(t)$ and $d_{\mathrm{c}}^{(\mathrm{R})}(t)$ is denoted by $g_{\mathrm{R}}(t)$; the impulse response that was obtained using $d_{\mathrm{b}}^{(\mathrm{L})}(t)$ and $d_{\mathrm{c}}^{(\mathrm{L})}(t)$ is denoted by $g_{\mathrm{L}}(t)$.

The impulse responses $g_{\mathrm{R}}(t)$ (radar) and $g_{\mathrm{L}}(t)$ (laser) for participants A and B are shown in Fig. 9, where the black and red lines represent $g_{\mathrm{R}}(t)$ and $g_{\mathrm{L}}(t)$, respectively. Notably, the impulse responses obtained using the radar system and the corresponding responses obtained using the laser sensors look alike; these responses show similar patterns, regardless of any individual differences. Because of the quasiperiodicity of these displacement waveforms, the impulse responses are also quasiperiodic. A significant negative trough can be seen around $\tau = 0$, which is then followed by double peaks. Interpretation of this impulse response shape will form part of the next step in our future research. This study focuses solely on the similarity between the impulse responses obtained using the radar system and the corresponding responses obtained using the laser sensors.

To enable evaluation of the similarity between $g_{\mathrm{R}}(t)$ and $g_{\mathrm{L}}(t)$, the normalized correlation of $\rho_g = \int g_{\mathrm{R}}(t) g_{\mathrm{L}}(t) \mathrm{d}t$ is calculated. The normalized maximum correlations for participants A, B, C, and D are $\rho_g = 0.94$, 0.97, 0.98, and 0.98 at time lags of $\tau = -3.0$, 11.0, 11.0, and -24.5 ms, respectively; the average correlation was as high as 0.97 and the average time lag error was 12.4 ms, which is sufficiently shorter than the typical PTT between the back and the calf. These results demonstrate the feasibility of the proposed radar-based noncontact approach to pulse wave propagation measurement. In future work, we intend to study the relationship between the impulse response $g_{\mathrm{R}}(t)$ and the related physiological parameters, e.g., BP and arterial stiffness, to enable the proposed method to be applied in healthcare systems.

IV. Discussion

A. Investigation of Repeatability

To verify the repeatability of our experimental accuracy evaluation, we performed additional measurements three more times for participant A. In the additional measurements, the correlation coefficients ρ_g between the impulse responses obtained from the radar and laser sensors were 0.92, 0.97, and 0.91. The average ρ_g (including the measurement in the previous section) for participant A was as high as 0.94, which suggests the repeatability of the accuracy evaluated in this study. In future, it will be important to perform additional large-scale measurements with more participants to verify the statistical repeatability of the proposed approach.

B. Advantage and Disadvantage of the Proposed Approach

Next, we discuss the advantages and disadvantages of the proposed approach. The advantages are described as follows. (1) Using the proposed approach, pulse wave propagation can be measured unobtrusively in a noncontact manner and without attachment of any sensors to the patient's body. (2) Using the proposed approach, the pulse wave propagation can be measured using only a single radar sensor, whereas many existing systems require multiple sensors (e.g., cuffs, electrodes, and radar sensors). (3) When using the proposed approach, pulse wave propagation can be measured through both clothes and bedding because MMWs penetrate these fabrics.

For contrast, the disadvantages of the proposed method are as follows. (1) The accuracy of the proposed approach is not necessarily as high as that of existing contact sensors. (2) The user is required to hold their breath for a few seconds during the measurement process. To mitigate the first disadvantage, we will study application of advanced signal processing techniques [35] to improve the signal separation accuracy. To resolve the second disadvantage, it will be necessary to develop an algorithm that can suppress the respiratory components from the radar signals, and this will form part of our future studies.

In this study, we used an operating frequency of 79 GHz, whereas the other radar-based studies [30]–[34] used lower frequencies (Table VII). The advantage of use of a 79-GHz radar system is related to its high sensitivity to small displacements; the skin displacement caused by a pulse wave is typically less than 100 μm, which corresponds to radar echoes with phase rotations of less than 19.0°, 5.8°, and 0.58° at frequencies of 79, 24, and 2.4 GHz, respectively. Therefore, in noisy data, the body displacement caused by a pulse wave is easier to detect at higher frequencies (e.g., at 79 GHz).

C. Comparison With Existing Studies

We discuss the uniqueness of the approach in this study. No existing studies have been reported to date that evaluated the accuracy of radar-based measurements of body

TABLE VII
COMPARISON WITH EXISTING STUDIES

Study	Frequency	No. of radars	No. of channels	Accuracy evaluation
Tang [30]	2.45 GHz	2	1	No
Lauteslager [31]	3.8 GHz	8	1	No
Vasireddy [32]	24 GHz	2	1	No
Lu [33]	6 GHz	2	1	No
Michler [34]	24 GHz	1	9	No
This study	79 GHz	1	12	Yes

displacements and pulse wave propagation quantitatively. For example, Michler *et al.* [34] used an array radar system and measured the displacement waveforms at two sites on the patient's abdomen. Vasireddy *et al.* [32] and Lu *et al.* [33] both used two radar systems and placed these systems close to the target body. However, none of these studies [32]–[34] reported evaluations of the accuracy of the measured displacements. In general, it is not easy to evaluate the accuracy of the measured displacements because placement of reference sensors on the body sites of interest can interfere with the radar measurements. Despite this, our proposed measurement setup, which is shown in Fig. 2, provided an evaluation of the accuracy of the displacement measurements. The number of radar systems and the number of antenna elements used in each of these studies are summarized in Table VII.

As explained in the Introduction, numerous studies have addressed the relationship between the BP and the pulse wave data when measured using contact-type sensors. Therefore, we did not reiterate the same processes in the data analysis; instead, we focused on the accuracy of estimation of the skin displacement waveforms in this study. Regardless of the above, it will be important to study the accuracy of noncontact BP measurements using the proposed approach, and this will also form part of our future studies.

Finally, we discuss the applicability of radar imaging to the identification of human body parts. Our measurement system can locate the reflection points on the human body and extract the displacement waveforms at those points, whereas the corresponding body parts are not identified. In the future, however, it will be important to obtain the entire shape of the human body using radar imaging [36]–[40] to allow the exact location of each beam spot to be estimated and the corresponding body parts identified.

V. CONCLUSION

In this study, we evaluated the accuracy of noncontact measurement of displacements in the human body caused by pulse wave propagation using a 79-GHz MMW UWB MIMO array radar system for the first time. A pair of laser displacement sensors was also used to measure the body displacement waveforms for reference in the evaluation of the proposed method. The DOAs of the echoes from two body parts were estimated by applying a beamformer method to the array radar signals and displacement waveforms were extracted from the back and the calf of each participant. By modeling the pulse wave propagation as a linear time-invariant system, the system's impulse response was calculated using the radar data and was then compared with the impulse response calculated using the laser data. The pulse wave impulse responses that were estimated using the radar and laser systems were evaluated quantitatively and compared. For the four participants (A, B, C, and D), the normalized correlation values between the impulse responses obtained from the radar and laser data ranged as high as 0.94, 0.97, 0.98, and 0.98, respectively. These experimental results demonstrated for the first time that arterial pulse wave propagation can be measured accurately in a noncontact manner using a single MIMO array radar system. This first report on the demonstration of these measurements is expected to lead to the development and realization of unobtrusive health monitoring systems to detect early-stage cardiovascular diseases in future work.

APPENDIX

The array factor $P_{\mathrm{A}}(\theta)$ for an N-element uniform antenna array with half-wavelength element spacings is given by

$$P_{\mathrm{A}}(\theta) = \left| \frac{\sin((N\pi/2)\sin\theta)}{N\sin((\pi/2)\sin\theta)} \right|^2, \tag{7}$$

where θ is the angle in the xz plane. The total beam pattern $P(\theta,\phi) = P_{\mathrm{A}}(\theta)P_{\mathrm{E}}(\theta,\phi)$ of the array is given by the product of the array factor $P_{\mathrm{A}}(\theta)$ and the element pattern $P_{\mathrm{E}}(\theta,\phi)$, where ϕ is the angle in the yz plane. In this study, the element pattern $P_{\mathrm{E}}(\theta,\phi)$ represents a fan-shaped beam with a narrow beamwidth within ϕ and a broad beamwidth within θ. Therefore, the beamwidths within the angles θ and ϕ of the total beam pattern $P(\theta,\phi)$ are mainly determined by the array factor $P_{\mathrm{A}}(\theta)$ and the element pattern $P_{\mathrm{E}}(\theta,\phi)$, respectively.

ETHICS DECLARATIONS

This study was approved by the Ethics Committee of the Graduate School of Engineering, Kyoto University (permit no. 201916). Informed consent was obtained from all participants in the study.

REFERENCES

[1] J. Blacher, A. P. Guerin, B. Pannier, S. J. Marchais, M. E. Safar, and G. M. London, "Impact of aortic stiffness on survival in end-stage renal disease," *Circulation*, vol. 99, no. 18, pp. 2434–2439, May 1999, doi: 10.1161/01.cir.99.18.2434.

[2] S. Meaume, A. Benetos, O. F. Henry, A. Rudnichi, and M. E. Safar, "Aortic pulse wave velocity predicts cardiovascular mortality in subjects >70 years of age," *Arteriosclerosis, Thrombosis, Vascular Biol.*, vol. 21, no. 12, pp. 2046–2050, Dec. 2001.

[3] S. Laurent, B. Kingwell, A. Bank, M. Weber, and H. Struijker-Boudier, "Clinical applications of arterial stiffness: Therapeutics and pharmacology," *Am. J. Hypertens.*, vol. 15, no. 5, pp. 453–458, May 2002, doi: 10.1016/s0895-7061(01)02329-9.

[4] J. Topouchian *et al.*, "Arterial stiffness and pharmacological interventions—The TRanscend arterial stiffNess Substudy (TRANS study)," *Vasc. Health Risk Manag.*, vol. 3, no. 4, pp. 381–387, Aug. 2007.

[5] S. S. Najjar *et al.*, "Pulse wave velocity is an independent predictor of the longitudinal increase in systolic blood pressure and of incident hypertension in the baltimore longitudinal study of aging," *J. Amer. College Cardiol.*, vol. 51, no. 14, pp. 1377–1383, Apr. 2008, doi: 10.1016/j.jacc.2007.10.065.

[6] *IEEE Standard for Wearable Cuffless Blood Pressure Measuring Devices*, Standard 1708-2014, 2014.

[7] R. A. Payne, C. N. Symeonides, D. J. Webb, and S. R. J. Maxwell, "Pulse transit time measured from the ECG: An unreliable marker of beat-to-beat blood pressure," *J. Appl. Physiol.*, vol. 100, no. 1, pp. 136–141, Jan. 2006, doi: 10.1152/japplphysiol.00657.2005.

[8] R. Mukkamala *et al.*, "Toward ubiquitous blood pressure monitoring via pulse transit time: Theory and practice," *IEEE Trans. Biomed. Eng.*, vol. 62, no. 8, pp. 1879–1901, Aug. 2015, doi: 10.1109/TBME.2015.2441951.

[9] J. Lass, I. C. Meigas, D. Karai, R. Kattai, J. Kaik, and M. Rossmann, "Continuous blood pressure monitoring during exercise using pulse wave transit time measurement," in *Proc. 26th Annu. Int. Conf. Eng. Med. Biol. Soc.*, San Francisco, CA, USA, Dec. 2004, pp. 2239–2242, doi: 10.1109/IEMBS.2004.1403652.

[10] T. Ma and Y. T. Zhang, "A correlation study on the variabilities in pulse transit time, blood pressure, and heart rate recorded simultaneously from healthy subjects," in *Proc. IEEE Eng. Med. Biol. 27th Annu. Conf.*, Shanghai, China, Jan. 2005, pp. 996–999, doi: 10.1109/IEMBS.2005.1616585.

[11] M. Y.-M. Wong, C. C.-Y. Poon, and Y.-T. Zhang, "An evaluation of the cuffless blood pressure estimation based on pulse transit time technique: A half year study on normotensive subjects," *Cardiovascular Eng.*, vol. 9, no. 1, pp. 32–38, Mar. 2009, doi: 10.1007/s10558-009-9070-7.

[12] Y. Zheng, B. P. Yan, Y. Zhang, C. M. Yu, and C. C. Y. Poon, "Wearable cuff-less PTT-based system for overnight blood pressure monitoring," in *Proc. 35th Annu. Int. Conf. Eng. Med. Biol. Soc. (EMBC)*, Osaka, Japan, Jul. 2013, pp. 6103–6106, doi: 10.1109/EMBC.2013.6610945.

[13] S. S. Thomas, V. Nathan, C. Zong, K. Soundarapandian, X. Shi, and R. Jafari, "BioWatch: A noninvasive wrist-based blood pressure monitor that incorporates training techniques for posture and subject variability," *IEEE J. Biomed. Health Informat.*, vol. 20, no. 5, pp. 1291–1300, Sep. 2016, doi: 10.1109/JBHI.2015.2458779.

[14] Y. Zheng, C. C. Y. Poon, B. P. Yan, and J. Y. W. Lau, "Pulse arrival time based cuff-less and 24-H wearable blood pressure monitoring and its diagnostic value in hypertension," *J. Med. Syst.*, vol. 40, no. 9, p. 195, Sep. 2016, doi: 10.1007/s10916-016-0558-6.

[15] C. Holz and E. J. Wang, "Glabella: Continuously sensing blood pressure behavior using an unobtrusive wearable device," *Proc. ACM Interact., Mobile, Wearable Ubiquitous Technol.*, vol. 1, no. 3, pp. 1–23, Sep. 2017, doi: 10.1145/3132024.

[16] D. B. McCombie, A. T. Reisner, and H. H. Asada, "Adaptive blood pressure estimation from wearable PPG sensors using peripheral artery pulse wave velocity measurements and multi-channel blind identification of local arterial dynamics," in *Proc. EMBS*, 2006, pp. 3521–3524, doi: 10.1109/IEMBS.2006.260590.

[17] S. L.-O. Martin *et al.*, "Weighing scale-based pulse transit time is a superior marker of blood pressure than conventional pulse arrival time," *Sci. Rep.*, vol. 6, no. 1, Dec. 2016, Art. no. 39273, doi: 10.1038/srep39273.

[18] J. Y. A. Foo, C. S. Lim, and P. Wang, "Evaluation of blood pressure changes using vascular transit time," *Physiol. Meas.*, vol. 27, no. 8, pp. 685–694, Aug. 2006, doi: 10.1088/0967-3334/27/8/003.

[19] Y.-P. Hsu and D. J. Young, "Skin-coupled personal wearable ambulatory pulse wave velocity monitoring system using microelectromechanical sensors," *IEEE Sensors J.*, vol. 14, no. 10, pp. 3490–3497, Oct. 2014, doi: 10.1109/JSEN.2014.2345779.

[20] Y.-J. Lee *et al.*, "Magneto-plethysmographic sensor for peripheral blood flow velocity," *IEEE Sensors J.*, vol. 14, no. 5, pp. 1341–1342, May 2014, doi: 10.1109/JSEN.2014.2304752.

[21] F. Heydari *et al.*, "Continuous cuffless blood pressure measurement using body sensors," in *Proc. IEEE Sensors*, New Delhi, India, Oct. 2018, pp. 1–4, doi: 10.1109/ICSENS.2018.8630294.

[22] H.-D. Lin, Y.-S. Lee, and B.-N. Chuang, "Using dual-antenna nanosecond pulse near-field sensing technology for non-contact and continuous blood pressure measurement," in *Proc. Ann. Int. Conf.*, San Diego, CA, USA, Aug. 2012, pp. 219–222, doi: 10.1109/EMBC.2012.6345909.

[23] D. Buxi, J.-M. Redoute, and M. R. Yuce, "Cuffless blood pressure estimation from the carotid pulse arrival time using continuous wave radar," in *Proc. 37th Annu. Int. Conf. Eng. Med. Biol. Soc. (EMBC)*, Milan, Italy, Aug. 2015, pp. 5704–5707, doi: 10.1109/EMBC.2015.7319687.

[24] D. Buxi, J.-M. Redout, and M. R. Yuce, "Blood pressure estimation using pulse transit time from bioimpedance and continuous wave radar," *IEEE Trans. Biomed. Eng.*, vol. 64, no. 4, pp. 917–927, Apr. 2017, doi: 10.1109/TBME.2016.2582472.

[25] D. Buxi *et al.*, "Systolic time interval estimation using continuous wave radar with on-body antennas," *IEEE J. Biomed. Health Informat.*, vol. 22, no. 1, pp. 129–139, Jan. 2018, doi: 10.1109/JBHI.2017.2731790.

[26] M. P. Ebrahim, F. Heydari, K. Walker, K. Joe, J.-M. Redoute, and M. R. Yuce, "Systolic blood pressure estimation using wearable radar and photoplethysmogram signals," in *Proc. IEEE Int. Conf. Syst., Man Cybern. (SMC)*, Bari, Italy, Oct. 2019, pp. 3878–3882, doi: 10.1109/SMC.2019.8914567.

[27] M. Pour Ebrahim *et al.*, "Blood pressure estimation using on-body continuous wave radar and photoplethysmogram in various posture and exercise conditions," *Sci. Rep.*, vol. 9, no. 1, Dec. 2019, Art. no. 16346, doi: 10.1038/s41598-019-52710-8.

[28] M. Kuwahara, E. Yavari, and O. Boric-Lubecke, "Non-invasive, continuous, pulse pressure monitoring method," in *Proc. 41st Annu. Int. Conf. IEEE Eng. Med. Biol. Soc. (EMBC)*, Berlin, Germany, Jul. 2019, pp. 6574–6577, doi: 10.1109/EMBC.2019.8857439.

[29] T.-H. Tao, S.-J. Hu, J.-H. Peng, and S.-C. Kuo, "An ultrawideband radar based pulse sensor for arterial stiffness measurement," in *Proc. 29th Annu. Int. Conf. IEEE Eng. Med. Biol. Soc.*, Lyon, France, Aug. 2007, pp. 1679–1682, doi: 10.1109/IEMBS.2007.4352631.

[30] M.-C. Tang, C.-M. Liao, F.-K. Wang, and T.-S. Horng, "Non-contact pulse transit time measurement using a single-frequency continuous-wave radar," in *IEEE MTT-S Int. Microw. Symp. Dig.*, Philadelphia, PA, USA, Jun. 2018, pp. 1409–1412, doi: 10.1109/MWSYM.2018.8439326.

[31] T. Lauteslager, M. Tommer, T. S. Lande, and T. G. Constandinou, "Coherent UWB radar-on-chip for in-body measurement of cardiovascular dynamics," *IEEE Trans. Biomed. Circuits Syst.*, vol. 13, no. 5, pp. 814–824, Oct. 2019, doi: 10.1109/TBCAS.2019.2922775.

[32] R. Vasireddy, J. Goette, M. Jacomet, and A. Vogt, "Estimation of arterial pulse wave velocity from Doppler radar measurements: A feasibility study," in *Proc. 41st Annu. Int. Conf. IEEE Eng. Med. Biol. Soc. (EMBC)*, Berlin, Germany, Jul. 2019, pp. 5460–5464, doi: 10.1109/EMBC.2019.8857644.

[33] L. Lu, C. Li, and D. Y. C. Lie, "Experimental demonstration of noncontact pulse wave velocity monitoring using multiple Doppler radar sensors," in *Proc. Annu. Int. Conf. IEEE Eng. Med. Biol.*, Buenos Aires, Argentina, Aug. 2010, pp. 5010–5013, doi: 10.1109/IEMBS.2010.5627213.

[34] F. Michler *et al.*, "Pulse wave velocity detection using a 24 GHz six-port based Doppler radar," in *Proc. IEEE Radio Wireless Symp. (RWS)*, Orlando, FL, USA, Jan. 2019, doi: 10.1109/RWS.2019.8714521.

[35] T. Sakamoto, "Signal separation using a mathematical model of physiological signals for the measurement of heart pulse wave propagation with array radar," *IEEE Access*, vol. 8, pp. 175921–175931, 2020, doi: 10.1109/ACCESS.2020.3026539.

[36] S. Bertl, A. Dallinger, and J. Detlefsen, "Interferometric focusing for the imaging of humans," *IET Radar, Sonar Navig.*, vol. 4, no. 3, pp. 457–463, Jun. 2010, doi: 10.1049/iet-rsn.2009.0029.

[37] Y. Alvarez, B. Gonzalez-Valdes, J. Ángel Martinez, F. Las-Heras, and C. M. Rappaport, "3D whole body imaging for detecting explosive-related threats," *IEEE Trans. Antennas Propag.*, vol. 60, no. 9, pp. 4453–4458, Sep. 2012, doi: 10.1109/TAP.2012.2207068.

[38] M. D. Buhari, G. Y. Tian, and R. Tiwari, "Microwave-based SAR technique for pipeline inspection using autofocus range-Doppler algorithm," *IEEE Sensors J.*, vol. 19, no. 5, pp. 1777–1787, Mar. 2019, doi: 10.1109/JSEN.2018.2879348.

[39] T. Sakamoto and T. Koda, "Respiratory motion imaging using 2.4-GHz Nine-Element-Array continuous-wave radar," *IEEE Microw. Wireless Compon. Lett.*, vol. 30, no. 7, pp. 717–720, Jul. 2020, doi: 10.1109/LMWC.2020.2992541.

[40] N. A. Salmon, "Indoor full-body security screening: Radiometric microwave imaging phenomenology and polarimetric scene simulation," *IEEE Access*, vol. 8, pp. 144621–144637, 2020, doi: 10.1109/ACCESS.2020.3013967.

Yuji Oyamada received the B.E. degree in electrical and electronic engineering from Kyoto University, Kyoto, Japan, in 2020, where he is currently pursuing the M.E. degree in electrical engineering with the Graduate School of Engineering.

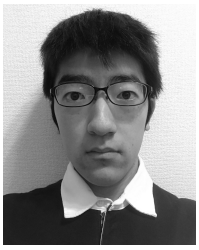

Takehito Koshisaka is currently pursuing the B.E. degree in electrical and electronic engineering with Kyoto University, Kyoto, Japan.

Takuya Sakamoto (Senior Member, IEEE) received the B.E. degree in electrical and electronic engineering from Kyoto University, Kyoto, Japan, in 2000, and the M.I. and Ph.D. degrees in communications and computer engineering from the Graduate School of Informatics, Kyoto University in 2002 and 2005, respectively.

From 2006 to 2015, he was an Assistant Professor with the Graduate School of Informatics, Kyoto University. From 2011 to 2013, he was a Visiting Researcher with the Delft University of Technology, Delft, The Netherlands. From 2015 to 2018, he was an Associate Professor with the Graduate School of Engineering, University of Hyogo, Himeji, Japan. In 2017, he was a Visiting Scholar with the University of Hawaii at Manoa, Honolulu, HI, USA. Since 2018, he has been a PRESTO Researcher with the Japan Science and Technology Agency, Kawaguchi, Japan. He is an Associate Professor with the Graduate School of Engineering, Kyoto University. His current research interests are system theory, inverse problems, radar signal processing, radar imaging, and wireless sensing of vital signs.

Dr. Sakamoto was a recipient of the Best Paper Award from the International Symposium on Antennas and Propagation (ISAP) in 2012 and the Masao Horiba Award in 2016. In 2017, he was invited as a semi-plenary speaker to the European Conference on Antennas and Propagation (EuCAP) in Paris, France.